

# Digital RNA sequencing minimizes sequence-dependent bias and amplification noise with optimized single-molecule barcodes

Katsuyuki Shiroguchi, Tony Z. Jia, Peter A. Sims, and X. Sunney Xie<sup>1</sup>

Department of Chemistry and Chemical Biology, Harvard University, Cambridge, MA 02138

Edited by Jonathan S. Weissman, University of California, San Francisco, CA, and approved December 14, 2011 (received for review November 1, 2011)

**RNA sequencing (RNA-Seq) is a powerful tool for transcriptome profiling, but is hampered by sequence-dependent bias and inaccuracy at low copy numbers intrinsic to exponential PCR amplification. We developed a simple strategy for mitigating these complications, allowing truly digital RNA-Seq. Following reverse transcription, a large set of barcode sequences is added in excess, and nearly every cDNA molecule is uniquely labeled by random attachment of barcode sequences to both ends. After PCR, we applied paired-end deep sequencing to read the two barcodes and cDNA sequences. Rather than counting the number of reads, RNA abundance is measured based on the number of unique barcode sequences observed for a given cDNA sequence. We optimized the barcodes to be unambiguously identifiable, even in the presence of multiple sequencing errors. This method allows counting with single-copy resolution despite sequence-dependent bias and PCR-amplification noise, and is analogous to digital PCR but amenable to quantifying a whole transcriptome. We demonstrated transcriptome profiling of *Escherichia coli* with more accurate and reproducible quantification than conventional RNA-Seq.**

systems biology | digital counting | next generation sequencing | gene expression | genomics

The central goal of transcriptome profiling is to accurately quantify the abundance of RNA transcripts in a sample. Although hybridization-based approaches like DNA microarrays can provide only a relative, analog measure of transcript abundance, sequencing-based approaches, such as RNA sequencing (RNA-Seq), have the advantage of removing hybridization bias among genes (1, 2) and offer the promise of true digital quantification.

The interpretation of conventional RNA-Seq is complicated by sequence-dependent bias and amplification noise from reverse transcription, adapter ligation, library amplification by PCR, solid-phase clonal amplification, and sequencing (3–5). NanoString technology mitigates these complications by eliminating enzymatic reactions and hybridizing color-coded probes directly to RNA for single-molecule detection (6), although it requires many specific probes. Other methods reduce bias in RNA-Seq by eliminating PCR and directly sequencing single molecules of RNA (7), or sequencing single molecules (8) or clonal populations (9) of cDNA. However, library amplification is desirable for sequencing small samples or single cells (10).

Conventional library amplification is based on PCR, but the exponential amplification afforded by PCR introduces noise, especially at low copy numbers (11). Digital PCR was introduced to circumvent this problem by distributing DNA molecules into many containers, each receiving zero or one molecules, which are amplified and detected by PCR (12). This technique has been successfully applied to RNA counting (13); however, it requires specific primers for each gene, which hinders high-throughput measurements.

Here we report a system-wide method for bias and noise reduction in RNA-Seq that allows the use of PCR to amplify a cDNA library before sequencing, providing accurate digital

quantification of the transcriptome. In our approach, each cDNA molecule is attached to a unique barcode sequence from a large pool of barcodes before amplification (Fig. 1A) (14). Deep sequencing then allows quantification of the number of cDNA molecules in the original sample by counting the number of unique barcode sequences associated with a given cDNA sequence. This concept has been applied recently for studying protein-RNA interactions (15), to improve the sensitivity of DNA mutation detection (16, 17) and accuracy of DNA copy-number measurements for individual genes by threshold detection (18), and to perform karyotyping and mRNA profiling (19). However, barcode identification in these studies was not immune to errors incurred during library preparation, amplification, and sequencing, which can convert one barcode into another. Hence, a substantial fraction of reads contained misidentified barcodes (16–19), which in some cases were discarded using an artificial threshold (17–19). To avoid this complication, we designed optimized barcodes that can be ligated and amplified with minimal bias and distinguished from one another despite the accumulation of PCR mutations and sequencing errors.

## Results

**Barcoding Strategy for Digital RNA-Seq.** Fig. 1A depicts the general concept of digital counting by random labeling of all target nucleic acid molecules in a sample with unique barcode sequences. To achieve unique barcoding of as many target sequences as possible, the set of barcode sequences introduced to the sample must be (i) much larger than the copy number of the most abundant target sequence and (ii) sampled randomly by the target sequences. If these two criteria are satisfied, then digital quantification of the target molecules by this method is limited only by sequencing depth and accuracy. Unlike conventional sequencing-based approaches to nucleic-acid quantification, the digital counting technique is no longer limited by intrinsic amplification noise and bias in downstream sample preparation and sequencing (Fig. 1A).

Implementation of the scheme in Fig. 1A for digital RNA-Seq requires several critical considerations. As noted above, if the barcode sequences are random, then a sequencing error at one position in a barcode will cause that barcode to be misidentified. This error-induced interconversion will occur even if the barcode sequences are nonrandom (18), unless the barcodes are carefully

Author contributions: K.S., T.Z.J., P.A.S., and X.S.X. designed research; K.S. and T.Z.J. performed research; K.S., T.Z.J., and P.A.S. analyzed the data; K.S., T.Z.J., P.A.S., and X.S.X. wrote the manuscript.

Conflict of interest statement: Harvard University has filed a provisional patent application based on this work.

This article is a PNAS Direct Submission.

Data deposition: The data reported in this paper have been deposited in the Gene Expression Omnibus (GEO) database, [www.ncbi.nlm.nih.gov/geo](http://www.ncbi.nlm.nih.gov/geo) (accession no. GSE34449).

<sup>1</sup>To whom correspondence should be addressed. E-mail: [xie@chemistry.harvard.edu](mailto:xie@chemistry.harvard.edu).

This article contains supporting information online at [www.pnas.org/lookup/suppl/doi:10.1073/pnas.1118018109/-DCSupplemental](http://www.pnas.org/lookup/suppl/doi:10.1073/pnas.1118018109/-DCSupplemental).

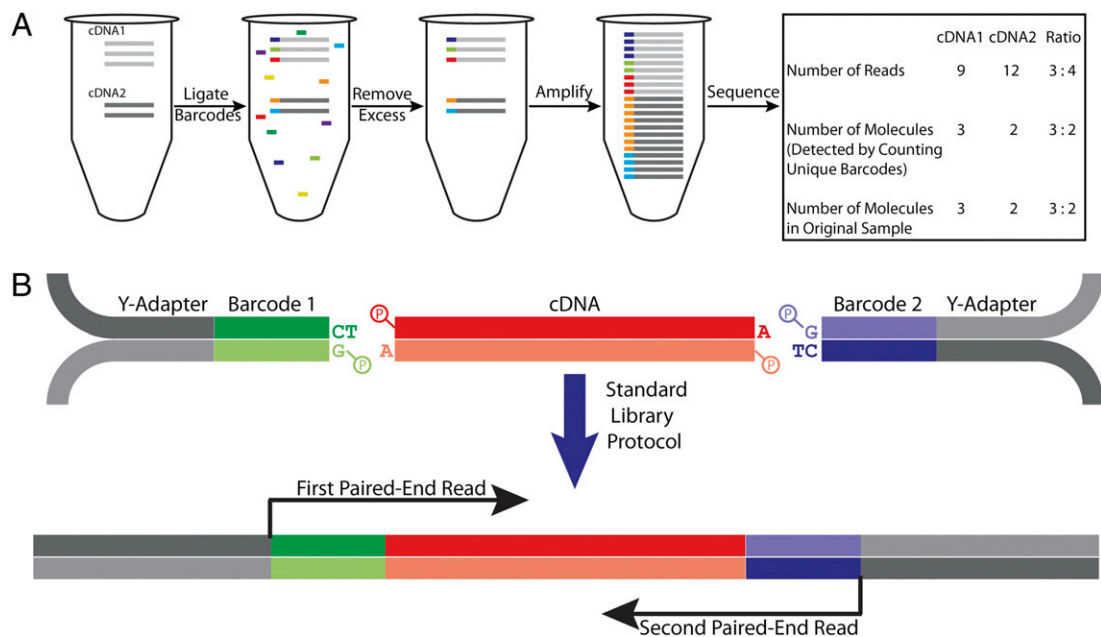


**Fig. 1.** Our scheme of digital RNA-Seq. (A) General principle of digital RNA-Seq. Assume the original sample contains two cDNA sequences, one with three copies and another with two copies. An overwhelming number of unique barcode sequences are added to the sample in excess, and five are randomly ligated to the cDNA molecules. Ideally, each cDNA molecule in the sample receives a unique barcode sequence. After removing the excess barcodes, the barcoded cDNA molecules are amplified by PCR. Because of intrinsic noise and sequence-dependent bias, the barcoded cDNA molecules are amplified unevenly. Consequently, after the amplicons are sequenced, it appears that there are three copies of cDNA1 for every four copies of cDNA2 based on the relative number of reads for each sequence. However, the ratio in the original sample was 3:2, which is accurately reflected in the relative number of unique barcodes associated with each cDNA sequence. (B) In our implementation of A, we found it advantageous to randomly ligate both ends of each phosphorylated cDNA fragment to a barcoded phosphorylated Illumina Y-shaped adapter. Note that the single T and A overhangs present on the barcodes and cDNA, respectively, are to enhance ligation efficiency. After this step, the sample is amplified by PCR and prepared for sequencing using the standard Illumina library protocol. For each amplicon, both barcode sequences and both strands of the cDNA sequence are read using paired-end deep sequencing.

designed so that multiple substitution errors and indels do not obscure their identities (20). Because DNA secondary structure can reduce amplification efficiency, the barcodes should not have significant sequence overlap or complementarity with each other, the adapter and primer sequences used in library preparation and sequencing, or the transcriptome-of-interest. Ideally, the barcode set will not contain sequence motifs that are known to be problematic for sequencing chemistries, such as long homopolymers and regions with high or low GC-content.

We used a computer program to generate a set of 145 barcode sequences 20-bp in length (Dataset S1) that satisfies the above criteria (*Materials and Methods* and *SI Materials and Methods*). The barcode sequences can sustain up to four substitution errors and remain unambiguously identifiable. In addition, a barcode that incurs up to nine substitution errors or the combination of one indel and five substitution errors will not take on the sequence of another barcode.

Instead of using a single barcode sequence to identify each target molecule in our sample (15–19), we attached a barcode sequence to both ends of each target molecule (Fig. 1B and *SI Materials and Methods*). If both ends of a target sequence sample all of the barcodes randomly, the target sequence will have access to  $145 \times 145 = 21,025$  unique labels. The two barcode sequences along with the target molecule sequence were then read out by paired-end sequencing (Fig. 1B). This paired-end strategy dramatically reduces the number of barcodes that must be designed and synthesized, is compatible with conventional paired-end library protocols, and provides long-range sequence information that improves mapping accuracy (21, 22). In addition, attaching barcodes to both ends increases the overall randomness of barcode sampling because the two ends of a target molecule are unlikely to have a similar degree of bias. We tested and characterized this

method on a set of quantified DNA spike-in sequences and a cDNA library derived from the transcriptome of *Escherichia coli*.

**Quantification of Spike-in Sequences and Barcode Sampling Bias.** To calibrate our digital RNA-Seq system, we measured the concentrations of five synthetic DNA spike-in sequences using the Fluidigm digital PCR platform and used them as internal standards. The spike-in samples were barcoded, added to the barcoded *E. coli* cDNA library, and quantified using the sequencing-based digital counting strategy described above. Fig. 2A shows that the number of digital counts (i.e., unique barcodes) observed in deep sequencing is well-correlated with the digital PCR calibration of the spike-in sequences.

To evaluate the difference between using random barcode sequences and our optimized barcode sequences, we conducted two experiments. In one experiment, we labeled the spike-in molecules with random barcode sequences (*SI Materials and Methods*), and in the second experiment we used our optimized, predetermined barcode set. We constructed the histograms of the number of reads for all barcodes observed from the most abundant spike-in sequence (Fig. 2B). When using random barcodes (red histogram in Fig. 2B and *SI Materials and Methods*), the left-most bin exhibits a large peak because a substantial fraction of barcodes are infrequently read because of sequencing errors; this causes barcodes to interconvert, generating quantification artifacts that were also evident in previous reports (16–19). In stark contrast, the left-most bin, when using optimized barcodes (green histogram in Fig. 2B), has no such peak because our optimized barcode sequences avoid misidentification because of sequencing errors. The effect of sequencing error on both random and optimized barcode counting is clearly shown by simulation (Fig. S1 and *SI Materials and Methods*).

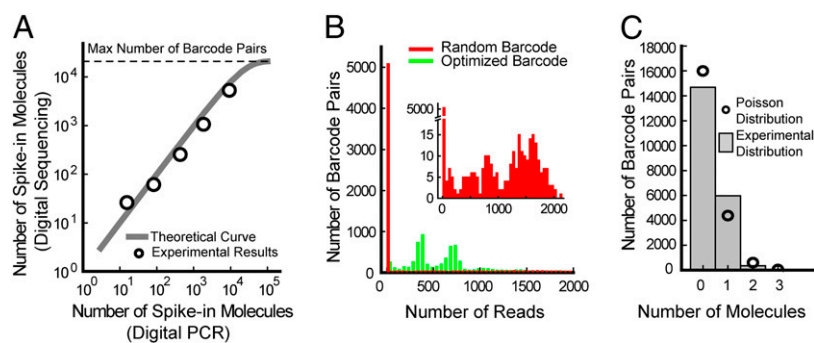


**Fig. 2.** Spike-in sequence quantification. (A) Correlation between the number of spike-in molecules for five different spike-in sequences as measured by digital PCR and digital counting of unique barcodes. The theoretical curve, which saturates because of the finite number of barcode pairs (21,025), is calculated based on the Poisson distribution (18). (B) Histograms of the number of reads corresponding to each observed barcode attached to the most abundant spike-in sequence for two experiments. The red histogram corresponds to a spike-in sequence labeled with random barcode sequences, and the green histogram corresponds to a spike-in sequence labeled with our optimized barcodes. Note the left-most bin in the red histogram is >10-times larger than that of the green histogram and contains a large number of unique barcodes with a low number of reads. This discrepancy is caused by various sequencing and PCR amplification errors, which generate new artifactual unique barcodes not present in the original sample and result in a large number of falsely identified unique barcodes (*SI Materials and Methods*). (Inset) The red histogram in greater detail. (C) Histogram of the number of times a barcode pair was observed with all five spike-in sequences (i.e., the number of spike-in molecules attached to a given barcode pair). Because the spike-in sequences sample the barcode pairs randomly with very little bias, the histogram follows a Poisson distribution.

We note that the green histogram in Fig. 2B is the distribution of the number of reads for the 5,311 uniquely barcoded molecules from a particular spike-in (*SI Materials and Methods*). Assuming each barcoded spike-in molecule is identical, the green histogram in Fig. 2B is essentially the probability distribution of the number of reads for a single molecule, which spans three orders-of-magnitude. This broad distribution arises primarily from intrinsic PCR amplification noise (11) in sample preparation. Given this broad single-molecule distribution, for low copy molecules in the original sample, counting the total number of reads (conventional RNA-Seq) would be catastrophic. On the other hand, this problem can be circumvented if one counts the number of different barcodes (integrated area of the histogram) using our digital RNA-Seq approach, yielding accurate quantification with single-copy resolution. The two counting schemes give the same results only when the copy number in the original sample is high, assuming there is no sequence-dependent bias.

Random sampling of the barcode sequences by each target sequence is essential for accurate digital counting. Fig. 2C shows that the distribution of observed molecule counts is in excellent agreement with Poisson statistics. Therefore, the five spike-in sequences sample the 21,025 barcode pairs without bias.

**Digital Quantification of the *E. coli* Transcriptome.** We obtained 26–32 million reads from our barcoded cDNA libraries that uniquely mapped to the *E. coli* genome (*Materials and Methods* and [Dataset S2](#)) in two replicate experiments. Fig. 3A shows the number of conventional and digital counts (unique barcodes) as a function of nucleotide position for the *fumA* transcription unit. Not surprisingly, the read density is considerably less uniform across the transcription unit than the number of digital counts, presumably because of intrinsic noise and bias in fragment amplification.

It is crucial for transcripts across the *E. coli* transcriptome to sample all barcodes evenly. Fig. 3B shows this distribution, which is close to Poisson but is somewhat overdispersed. Such biased sampling reduces the effective number of barcode sequences  $N_{\text{eff}}$  available. However, in our *E. coli* transcriptome sample, the copy number of the most abundant cDNA ranges from 10 to 40 copies for both counting methods. Based on Poisson statistics, even for the most abundant cDNA fragments in our sample, the required  $N_{\text{eff}}$  is  $\sim 100$ –400 for 95% unique labeling of all molecules (18). Because there are 21,025 barcode pairs available, on average the degree of randomness observed in Fig. 3B is sufficient.

The conventional method counts the number of amplicons, a quantity that is subject to bias and intrinsic amplification noise (11), rather than the number of molecules in the original sample. Conversely, in our digital counting scheme, unique barcode sequences distinguish each molecule in the sample, and so the effects of intrinsic noise are minimized. Fig. 3C shows how drastically different digital counting can be from conventional counting at low copy numbers, implying that digital counting of unique barcodes is advantageous, particularly for quantifying low copy fragments. We note that the correlation is stronger for high copy fragments and the same phenomenon is also observed for whole transcription units and genes ([Fig. S2](#)).

To demonstrate the superior accuracy of digital counting, we examined the uniformity of our abundance measurements within individual transcripts. Because individual transcription units were, by-and-large, intact RNA molecules following RNA synthesis, the cDNA fragments that map to one region of a given transcription unit should have the same abundance as fragments that map to a different region of the same transcription unit. We histogrammed the ratio between the variation in conventional counting  $\nu_C$  and variation in digital counting  $\nu_D$  for transcription units in different abundance ranges ([Fig. 3D](#)). A variation ratio of  $\nu_C/\nu_D = 1$  indicates that both conventional and digital counting give similarly uniform abundances along the length of a transcription unit. For a transcription unit where  $\nu_C/\nu_D$  exceeds one, conventional counting measures abundance less consistently along the transcription unit than digital counting. The mean values of  $\nu_C/\nu_D$  in the two replicates are 1.4 ( $s = 1.5$ , where  $s$  is sample SD) and 1.2 ( $s = 0.5$ ) for the complete set of analyzed transcription units, indicating that conventional counting is less consistent than digital counting across an average transcription unit. Furthermore, the mean value of  $\nu_C/\nu_D$  increases with decreasing copy number and its distribution becomes broader ([Fig. 3D](#)). For transcription units in the lowest abundance regime, the mean values of  $\nu_C/\nu_D$  are 1.9 ( $s = 2.4$ ) and 1.3 ( $s = 0.9$ ) for the two replicates. We conclude that, on average, digital counting outperforms conventional counting in terms of accuracy, and its performance advantage is most pronounced for low abundance transcription units.

Although Fig. 3 demonstrates that digital counting is less noisy and more accurate than conventional counting, Fig. 4 shows that digital counting is also more reproducible. We demonstrate this on the level of a single transcription unit in Fig. 4A, which shows

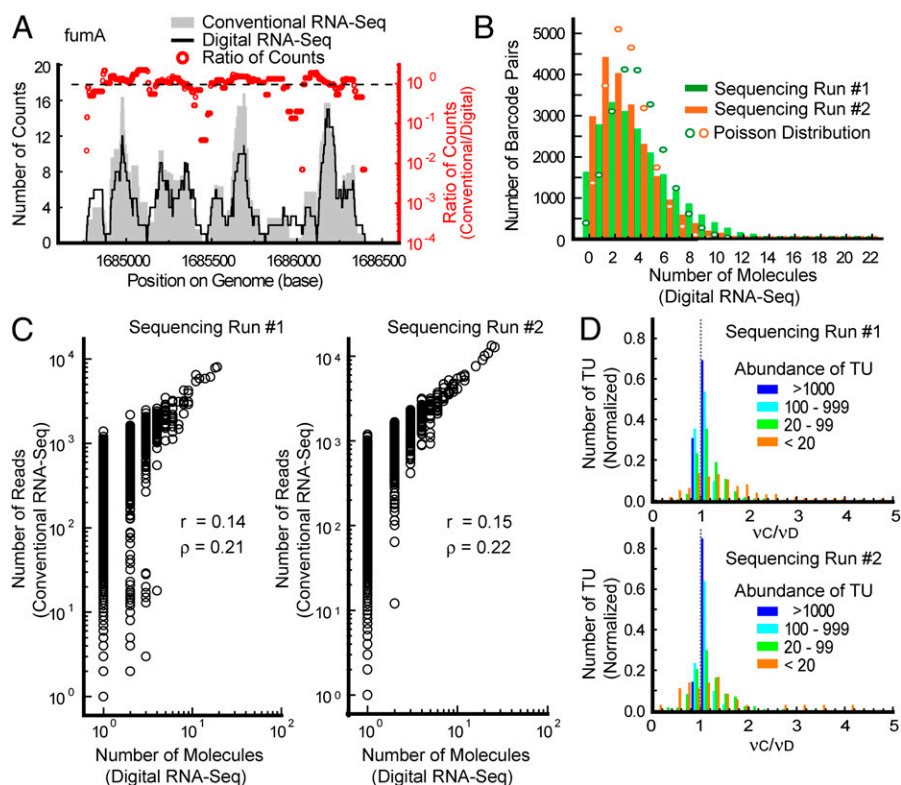


**Fig. 3.** Digital quantification of the *E. coli* transcriptome. (A) Conventional and digital counting results for the *fumA* transcription unit (TU) as a function of genome position. The conventional counts were calculated by using a conventional calibration curve that allows regression of the number of reads against the number of input molecules for all spike-in molecules (Fig. 2A). The digital counts were obtained by counting the number of unique barcodes associated with each fragment. The red dots are the ratios of these two numbers for each base. (B) Histograms of the number of times a barcode pair was observed with the *E. coli* cDNA sequences (i.e., the number of cDNA molecules attached to a given barcode pair) in the two replicates. Barcode sampling is more biased on average for *E. coli* cDNA fragments, but is still in reasonably good agreement with Poisson statistics. (C) Correlation between the number of reads (conventional counting) and the number of molecules obtained from digital counting of unique barcodes for every mapped fragment in the two replicates. For low copy molecules, the conventional counts are distributed over three orders-of-magnitude; this is because the conventional method counts amplicons, which are subject to intrinsic noise (11), rather than directly counting molecules in the original samples like the digital counting method. We note that higher copy fragments are less affected by intrinsic noise (11), as the number of molecules sequenced is greater; this effectively allows averaging over the read counts of many molecules in conventional RNA-Seq, decreasing the variance of counting in the process. (D) Uniformity of conventional vs. digital counting along the length of each transcription unit as a function of transcription unit abundance across the whole *E. coli* transcriptome for both replicates. We calculated the variation  $v_D = s_D/\mu_D$  (where  $\mu_D$  and  $s_D$  are the mean and sample SD of the digital counts among 99-base bins in a transcription unit, respectively) associated with digital counting and the variation  $v_C = s_C/\mu_C$  associated with conventional counting within each transcription unit for which at least three bins contained on average at least one read. We then created the histogram of the ratio between conventional and digital counting variation ( $v_C/v_D$ ) for transcription units in different abundance ranges for each replicate. Transcription unit abundance is the sum of all digital counts for each fragment in the transcription unit.

the ratio of counts between the two replicates for both conventional and digital counting along the *fumA* transcript. This ratio is consistently close to one for digital counting, but fluctuates over three orders-of-magnitude for conventional counting. We analyzed the global reproducibility of the whole transcriptome for quantification of transcription units and genes for both conventional and digital counting in Fig. 4 B and C, respectively. In both cases, the correlation between replicates is noticeably better for digital counting than conventional counting, particularly for low copy transcripts.

## Discussion

Unlike previously reported methods of eliminating bias and noise from RNA-Seq (7–9), our strategy allows amplification by PCR and uses standard commercial protocols for sample preparation. However, the implementation described above also leaves considerable room for improvement. For example, one could ligate barcoded adapters directly to RNA (23, 24), reducing the bias that occurs during reverse transcription. Alternatively, a recently described protocol for processing mature mRNA from single mammalian cells could be modified to include barcoded primers

for reverse transcription and second-strand synthesis before amplification (10), obviating the need for ligation.

One disadvantage of our technique is that it requires higher sequencing coverage than conventional RNA-Seq. This requirement is because both the transcriptome and the barcode set must be evenly sampled for accurate counting. However, the cost-per-base of deep sequencing continues to decrease rapidly. In our experiment, the mean number of reads per fragment was  $\sim 400$ . However, the spike-in sequencing reads can be randomly down-sampled 10-fold (*SI Materials and Methods*) without perturbing the correlation between abundance measured by digital PCR and digital barcode counting (Fig. S3), which implies that significantly lower coverage will suffice in many cases.

For applications where many cycles of PCR are required for sensitive detection, bias and noise reduction are crucial for accurate quantification. Although we demonstrated our technique on the *E. coli* transcriptome, we note that the maximum copy number for polyadenylated mRNA in a single mouse blastomere was found to be  $\sim 2,400$  (10). With 155 optimized barcode sequences (10 more than were used in this study), one could uniquely label nearly every identical molecule in this system



**ACKNOWLEDGMENTS.** Illumina sequencing was performed at the Harvard Faculty of Arts and Sciences Center for Systems Biology, with the help of Christian Daly, and at the Tufts University School of Medicine Genomics Core Facility, with the help of Kip Bodi and James Schiemer; digital PCR was performed by the Fluidigm Genetic Analysis Facility at the Molecular Genetics Core Facility of the Children's Hospital Boston Intellectual and Developmental Disabilities Research Center, with the help of Hal Schneider and Ta-Wei Lin; and base-calling analysis was performed at the Harvard

Faculty of Arts and Sciences Research Computing Group by Jiangwen Zhang. This work was supported by National Institutes of Health (NIH) National Human Genome Research Institute Grant HG005097-01 (to X.S.X.) and NIH National Human Genome Research Institute Recovery Act Grand Opportunities Grant 1RC2HG005613-01 (to X.S.X.); and K.S. was supported by a Postdoctoral Fellowship for Research Abroad from the Japanese Society for the Promotion of Science and a fellowship from The Uehara Memorial Foundation.

- Mortazavi A, Williams BA, McCue K, Schaeffer L, Wold B (2008) Mapping and quantifying mammalian transcriptomes by RNA-Seq. *Nat Methods* 5:621–628.
- Nagalakshmi U, et al. (2008) The transcriptional landscape of the yeast genome defined by RNA sequencing. *Science* 320:1344–1349.
- Dohm JC, Lottaz C, Borodina T, Himmelbauer H (2008) Substantial biases in ultra-short read data sets from high-throughput DNA sequencing. *Nucleic Acids Res* 36:e105.
- Aird D, et al. (2011) Analyzing and minimizing PCR amplification bias in Illumina sequencing libraries. *Genome Biol* 12:R18.
- Zheng W, Chung LM, Zhao H (2011) Bias detection and correction in RNA-Sequencing data. *BMC Bioinformatics* 12:290.
- Geiss GK, et al. (2008) Direct multiplexed measurement of gene expression with color-coded probe pairs. *Nat Biotechnol* 26:317–325.
- Ozsolak F, et al. (2009) Direct RNA sequencing. *Nature* 461:814–818.
- Lipson D, et al. (2009) Quantification of the yeast transcriptome by single-molecule sequencing. *Nat Biotechnol* 27:652–658.
- Mamanova L, et al. (2010) FRT-seq: amplification-free, strand-specific transcriptome sequencing. *Nat Methods* 7:130–132.
- Tang F, et al. (2009) mRNA-Seq whole-transcriptome analysis of a single cell. *Nat Methods* 6:377–382.
- Peccoud J, Jacob C (1996) Theoretical uncertainty of measurements using quantitative polymerase chain reaction. *Biophys J* 71:101–108.
- Vogelstein B, Kinzler KW (1999) Digital PCR. *Proc Natl Acad Sci USA* 96:9236–9241.
- Ottesen EA, Hong JW, Quake SR, Leadbetter JR (2006) Microfluidic digital PCR enables multigene analysis of individual environmental bacteria. *Science* 314:1464–1467.
- Hug H, Schuler R (2003) Measurement of the number of molecules of a single mRNA species in a complex mRNA preparation. *J Theor Biol* 221:615–624.
- Chi SW, Zang JB, Mele A, Darnell RB (2009) Argonaute HITS-CLIP decodes microRNA-mRNA interaction maps. *Nature* 460:479–486.
- Casbon JA, Osborne RJ, Brenner S, Lichtenstein CP (2011) A method for counting PCR template molecules with application to next-generation sequencing. *Nucleic Acids Res* 39:e81.
- Kinde I, Wu J, Papadopoulos N, Kinzler KW, Vogelstein B (2011) Detection and quantification of rare mutations with massively parallel sequencing. *Proc Natl Acad Sci USA* 108:9530–9535.
- Fu GK, Hu J, Wang PH, Fodor SP (2011) Counting individual DNA molecules by the stochastic attachment of diverse labels. *Proc Natl Acad Sci USA* 108:9026–9031.
- Kivioja T, et al. (2011) Counting absolute numbers of molecules using unique molecular identifiers. *Nat Methods*, 10.1038/nmeth.1778.
- Hamady M, Walker JJ, Harris JK, Gold NJ, Knight R (2008) Error-correcting barcoded primers for pyrosequencing hundreds of samples in multiplex. *Nat Methods* 5: 235–237.
- Wang Z, Gerstein M, Snyder M (2009) RNA-Seq: A revolutionary tool for transcriptomics. *Nat Rev Genet* 10:57–63.
- Au KF, Jiang H, Lin L, Xing Y, Wong WH (2010) Detection of splice junctions from paired-end RNA-seq data by SpliceMap. *Nucleic Acids Res* 38:4570–4578.
- Lau NC, Lim LP, Weinstein EG, Bartel DP (2001) An abundant class of tiny RNAs with probable regulatory roles in *Caenorhabditis elegans*. *Science* 294:858–862.
- Axtell MJ, Jan C, Rajagopalan R, Bartel DP (2006) A two-hit trigger for siRNA biogenesis in plants. *Cell* 127:565–577.
- Core LJ, Waterfall JJ, Lis JT (2008) Nascent RNA sequencing reveals widespread pausing and divergent initiation at human promoters. *Science* 322:1845–1848.
- Churchman LS, Weissman JS (2011) Nascent transcript sequencing visualizes transcription at nucleotide resolution. *Nature* 469:368–373.
- Ingolia NT, Ghaemmaghami S, Newman JR, Weissman JS (2009) Genome-wide analysis in vivo of translation with nucleotide resolution using ribosome profiling. *Science* 324:218–223.
- Alon S, et al. (2011) Barcoding bias in high-throughput multiplex sequencing of miRNA. *Genome Res* 21:1506–1511.
- Johnson DS, Mortazavi A, Myers RM, Wold B (2007) Genome-wide mapping of in vivo protein-DNA interactions. *Science* 316:1497–1502.
- Nix DA, et al. (2008) Empirical methods for controlling false positives and estimating confidence in ChIP-Seq peaks. *BMC Bioinformatics* 9:523.
- Ozsolak F, et al. (2010) Amplification-free digital gene expression profiling from minute cell quantities. *Nat Methods* 7:619–621.
- Shah SP, et al. (2009) Mutation of *FOXO2* in granulosa-cell tumors of the ovary. *N Engl J Med* 360:2719–2729.
- Bentley DR, et al. (2008) Accurate whole human genome sequencing using reversible terminator chemistry. *Nature* 456:53–59.
- Keseler IM, et al. (2011) EcoCyc: A comprehensive database of *Escherichia coli* biology. *Nucleic Acids Res* 39(Database issue):D583–D590.